Monochromatic aberrations of human eyes in the horizontal visual field

David A Atchison and Dion H Scott

Centre for Eye Research, School of Optometry, Queensland University of Technology,

Kelvin Grove, Q 4059, Australia

ABSTRACT

We measured the monochromatic aberrations of five subjects' right eyes both temporally and nasally out to 40 degrees from fixation. We used a Hartmann-Shack sensor, with modifications to equipment and software to enable off-axis measurements. Results were standardized for 6mm pupils. There were considerable variations between subjects in the pattern of aberrations. Aberrations were generally greater in the nasal visual field than in the temporal visual field; in the case of third-order aberrations, this was true for all subjects. The contribution of third-order Zernike aberrations to the root-mean squared aberration increased up to 4 times from the central to the edge of the field, but the contribution of 4th to 6th order Zernike aberrations varied little across the visual field. Results were similar to a previous investigation using laser raytracing, and were of the order of those predicted by Navarro's finite schematic eye.

OCIS codes: 080.3620 (lens design), 330.4460 (ophthalmic optics), 330.5370 (physiological optics)

1.   INTRODUCTION

The optics associated with the peripheral retina is poor, largely because of focusing errors in the form of oblique astigmatism and field curvature. A number of studies have measured these aberrations, which when converted to longitudinal aberrations, amount to several diopters[1-8]. When the periphery is carefully refracted the image quality improves considerably[9-12].

Little is known about how other aberrations such as spherical-like aberrations and coma-like aberrations vary across the field of vision e.g. do these remain unchanged or increase dramatically with increase in off-axis angle? If they do increase, they may also be significant for visual performance with large pupil sizes. Navarro *et al.*[13] used their laser ray tracing technique to determine these aberrations for 4 subjects out to 40 degrees in the nasal visual field. A narrow laser beam scanned the eye, and the direction of the reflected light gave the transverse aberrations that were converted into wave aberrations. The root-mean-square of the Zernike wave aberrations higher than the second order increased by a factor of two from fixation out to 40° (6.7 mm diameter pupil). This suggests that the variation in the higher order aberrations is not dramatic across the visual field.

We have extended the work of Navarro *et al.* by measuring the peripheral aberrations of the right eyes of five subjects both temporally and nasally along the horizontal meridian using a modified Hartmann-Shack wavefront sensor technique.

2. METHODS

2.1 Subjects

Subjects were the two authors and three additional subjects. Ages ranged from 31 to 47 years. Only right eyes were used. Spherical equivalent corrections ranged from +1.50DS to –2.00DS, and on-axis astigmatism was 0.75D or less for all subjects. Eyes were dilated with 1% cyclopentolate.

2.2 Hartmann-Shack sensor aberrometry

Figure 1 shows the apparatus. Light from a 543nm HeNe Laser was spatially filtered and collimated to pass through 1mm diameter aperture A_1, relay lens pair L_1 and L_2, and into the eye. Exposure time was 0.5s. Radiant flux in the pupil plane was 8 μW, which gives a safety factor of 100 times[14]. Fixation target 1 was used for on-axis vision. A bitebar, positioning equipment, infra-red illumination ring and video-camera allowed the eye to be correctly positioned in three dimensions. The eye and lens L_2 acted as a Badal lens system that could be moved to manipulate focus. Light reflected from the retina passed through two pairs of relay lenses (L_2-L_3 and L_4-L_5), though aperture A_3, the Hartmann-Shack wave sensor HSWS, and onto a Microview CCD camera. A_3 was conjugate with the retina, and was kept as small as possible to reduce corneal reflection while letting all light from the retina through to the camera. Two crossed polaroids helped also to minimise reflection. Wavefront sensor HSWS was conjugate with the eye pupil, and had a rectangular array of 0.4mm diameter micro-lenses of focal length 24mm (0400-24-S, Adaptive Optics Associates). Because of the limited size of the CCD array (8.98 x 7.2mm), in order to fully sample the aberrations for large pupils, the focal length of L_4 was 120mm as compared with 100mm for L_5, thus providing a magnification from the eye pupil onto the sensor of 0.833. This altered transverse aberration corresponding to any pupil position, by the same factor. However, wave aberration was unaffected as this is proportional to the rate of change of transverse aberration with change in exit pupil position (equation (1)).

We determined centroids of images using a graphics user interface utility for enhancing and segmenting images.

It was then necessary to match the centroids with those of a reference image. The latter was obtained near the time that the eye image was taken, by using a plane mirror in the position of the eye. This reference image was used, rather than an ideal image, to compensate for any small aberrations in the optical system. Corresponding centroids between the aberrated eye image I_{eye} and the reference image I_{ref} were matched, based on the assumption that local changes in the aberrated wavefront slope were sufficiently small that neighbouring spot locations did not cross over. The algorithm performing this automatic matching began by determining the geometric center of all centroids in I_{eye}. The centroid (x_{ref}, y_{ref}) nearest this geometric center in I_{ref} was found. All the points in the eye image were sorted in ascending order in terms of their Euclidean distance from (x_{ref}, y_{ref}). This ordering determined the sequence in which the points in I_{eye} were matched with those in I_{ref}, which was from the (approximate) center of the pupil outwards. Working through this sequence, the Euclidean distances between a given centroid in I_{eye} and all those in I_{ref} were found. The reference centroid that formed the smallest distance, which had not been matched previously, was matched with that from I_{eye}. Once matching was completed, the pupil radius was determined. The radius was not calculated from I_{eye}, as the positions of its points were aberrated, but from the corresponding points in the non-aberrated I_{ref}. The process began by finding the convex hull of the matched reference centroids. An eccentric ellipse was fitted in a least squares fit to this set, and from it the pupil center was determined. The pupil radius was the maximum Euclidean distance between the pupil center and all of the matched reference centroids. If we wanted to use a smaller pupil size, which was 3mm radius or 6mm diameter in this study, we started from the determined pupil center and found the subset of reference centroids within the selected pupil.

The local slopes, or partial derivatives, of the wavefront were determined from centroids (x_a, y_a) of the spots on the CCD camera relative to the sampling co-ordinates (x, y) on the Hartmann-Shack array. Formally,

$$\frac{\partial W(x, y)}{\partial x} = -\frac{\Delta x}{f}, \ \frac{\partial W(x, y)}{\partial y} = -\frac{\Delta y}{f} \qquad (1)$$

where f is the focal length of the micro-lenses, and

$$\Delta x = x - x_a, \Delta y = y - y_a \qquad (2)$$

Co-ordinates (x, y) were obtained from the reference image.

Zernike wavefront aberration polynomials[15] were obtained using a least squares regression. An F-test optimisation routine determined the number of Zernike orders to be used in the fit. Regardless of the fit order indicated, which varied between 4 and 10, a minimum of 6 orders was used so that aberrations could be compared up to the 6th order for all subjects and visual field positions.

2.2.1 *Modifications for peripheral vision*

For off-axis aberration measurements, the eye rotated either to right or left. Fixation target 2 was viewed directly for sufficiently large angles for which it could be seen unimpeded, but otherwise it was viewed through mirror PBS$_3$ (Figure 1). The target was carefully positioned so that the angle was correct. In this configuration, the wavefront sensor remains parallel to the (unaberrated) wavefront.

Measurements were taken in 5° intervals between (-)40° temporal visual field (nasal retina) and (+)40° degrees nasal visual field (temporal retina). Usually three images were taken at each off-axis angle. The image quality corresponding to off-axis vision was sometimes poor, chiefly because of field curvature and oblique astigmatism and it was often necessary to change focus by moving the eye and L$_2$ together. Defocus was later corrected to the emmetropic focus setting.

Zernike polynomials apply to circular pupils, but off-axis fixation changes these pupils to be close to elliptical pupils as viewed from the Hartmann-Shack array. To ensure that the assumption of circular pupils was maintained, in the procedure to match the spots between the aberrated eye image I_{eye} and the reference image I_{ref}, the eccentric centroid data was transformed into one that was circular, which required stretching the x-axis coordinates of the centroids by an amount equal to $1/\cos(\theta)$, where θ was the angle of rotation. x-axis co-ordinates of the Hartmann-Shack array sampling positions and their aberrated positions (x and x_a, respectively, in equation (2)) became

$$x' = x/\cos(\theta), \; x'_a = x_a/\cos(\theta) \tag{3}$$

This means that fewer points are being sampled as rotation angle increases for a given pupil size.

The pupil radius was determined from the set of modified sampling coordinates (x', y) whose convex hull should now approach a circle. When calculating the lateral shifts, $\Delta x = x' - x'_a$, $\Delta y = y - y_a$, between sampling and aberrated spot positions, the x-axis shifts must be corrected for the elongation of their co-ordinates made previously by multiplying them by a factor of $\cos(\theta)$. We must multiply the x-axis lateral shifts by a further $\cos(\theta)$ to reduce the effective wavefront slope by a factor equal to the eye's rotation, because the off-axis wavefront is being measured as though it was on-axis. Thus, the lateral shifts used to calculate the local slopes of the wavefront were

$$\Delta x = (x' - x'_a)\cos^2(\theta), \; \Delta y = (y - y_a) \tag{4}$$

from which the partial derivatives of the wavefront were calculated by

$$\frac{\partial W(x', y)}{\partial x'} = -\frac{\Delta x}{f}, \; \frac{\partial W(x', y)}{\partial y} = -\frac{\Delta y}{f} \tag{5}$$

2.3 Other raytracing

Further raytracing was done into and out of the eye with the unaccommodated variant of Navarro's finite model eye[16,17]. It has reasonable mean estimates of on- and off-axis aberrations of real eyes[17,18].

3.   RESULTS

Figures 2a-e shows root-mean-squared aberrations of Zernike aberration orders for subjects. For each subject, defocus has been modified by the same amount at each visual field angle so that it is zero on-axis. The most noted feature is the asymmetry between temporal and nasal fields for each subject, with the nasal fields generally having the higher aberrations. Note the peaks of the 2nd order aberrations at 15° temporal in Figures 2b and c caused by the optic discs. Considerable differences occur between the subjects, particularly for the dominating 2nd order aberrations. All subjects show increases in 3rd order aberrations away from the center of the visual field that are greater for the nasal than for the temporal visual field, there is no strong change in the 4th order aberration magnitude across the field, and 5th and 6th order aberrations are low relative to 3rd and 4th order aberrations.

The mean root-mean-squared aberrations are shown in Figure 2f. The dominating 2nd order aberrations have been removed and the vertical scale is different from that of Figure 2a-e. The -35° and +35° degree results have not been used as data were taken for only 2 subjects, and the data for +40° are based on only 3 subjects (DAA, DS, LS) because the other two subjects' images were too poor to analyse. The mean 3rd order aberrations change by 3 times for the temporal field and to 5 times for the nasal field. As noted previously, the 4th order contribution changes little across the visual field and the magnitude of the 5th and 6th orders are small by comparison with the 3rd and 4th orders.

For comparison with our results, we show the 3rd-5th order aberrations of Navarro *et al.*[13] using laser raytracing along the nasal semi-meridian in Figure 3a. The Navarro results were specified as being for 6.72mm pupils, although the centers of the spots going into the eye give a dimension of 6mm. Levels of 3rd order aberration are similar in the two studies, although Navarro *et al.* had slightly the greater coma in the center of the field and somewhat less in the periphery so that they obtained 2.5 times variation compared with 4.6 times in our study (Figure 2f). Navarro *et al.* had 2.8 times increase in 4th order aberrations across the visual field whereas we found little change. Navarro found an increase in 5th order across the nasal field, which is higher than we found. It must be remembered that both studies contained only a few subjects.

Figure 3b shows 3rd-6th order experimental aberrations for Navarro's model eye using a 6mm entrance pupil on-axis (stop diameter 5.39mm). No noticeable difference in results occurred for tracing into or out of the eye. As this model is rotationally symmetrical, neither 3rd nor 5th order aberrations occur on-axis. Navarro's model predicts a linear increase in coma with increase in angle, which is greater than our mean value by 10° nasal, and is about 30% greater than our results by 40° nasal. It shows an increase in 4th order aberrations, which we did not find, of 2.1 times. Its 5th and higher order aberrations are negligible.

4. DISCUSSION

Monochromatic aberrations of the eye that can be corrected by ophthalmic lenses (2nd order aberrations) have been long studied. Navarro *et al.*[13] provided the first measure of off-axis higher order aberrations by using a laser raytracing technique. This was done for the nasal semi-meridian of four eyes. They found substantial 3rd order aberrations that increased with visual field angle. We have reported a study involving 5 eyes, both directions along the horizontal meridian, and a modified version of the Hartmann-Shack technique. We obtained similar results to Navarro *et al.*, but found higher mean levels of 3rd order aberrations in the nasal visual field and substantial asymmetry in all subjects such that the 3rd order aberrations were higher in the nasal visual field than in the temporal visual field for all our subjects. Second order aberrations were highly asymmetric, a finding which has been observed frequently in the past[1-8]. For a pupil size of 6mm, aberrations of order higher than the 4th contributed little in normal eyes to the overall aberrations out to at least ±40°.

We could not measure aberrations at +40° in two of five subjects because of poor image quality. Improvements could be obtained by placing auxiliary cylindrical lenses conjugate to the eye's pupil at A_2 in Figure 1, or by using a Hartmann-Shack sensor with a shorter focal length.

Our aberrations were of the order of those of the unaccommodated form of Navarro's schematic eye, and demonstrate again that it provides good approximations to aberrations of real eyes.

5. ACKNOWLEDGEMENTS

6. REFERENCES

1. C. E. Ferree, G. Rand and C. Hardy, "Refraction for the peripheral field of vision," Arch Ophthal. **9**, 925-938 (1931).

2. C. E. Ferree, G. Rand and C. Hardy, "Refractive asymmetry in the temporal and nasal halves of the visual field," Am. J. Ophthal. **15**, 513-522 (1932).

3. C.E. Ferree and G. Rand, "Interpretation of refractive conditions in the peripheral field of vision," Arch. Ophthal. 5, 717-731 (1933).

4. T. C. A. Jenkins, "Aberrations of the eye and their effects on vision: Part 2," Br. J. Physiol. Opt. **20**, 161-201 (1963).

5. F. Rempt, J. Hoogerheide and W. P. H. Hoogenbloom, "Peripheral retinoscopy and the skiagram," Ophthalmologica **162**, 1-10 (1971).

6. M. Millodot, "Effect of ametropia on peripheral refraction," Am. J. Optom. Physiol. Opt. **82**, 461-465 (1981).

7. G. Smith, M. Millodot and N. McBrien, "The effect of accommodation on oblique astigmatism and field curvature of the human eye," Clin. Exp. Optom. **71**, 119-125 (1988).

8. J. Gustafsson, E. Terenius, J. Buchheister and P. Unsbo, "Peripheral astigmatism in emmetropic eyes," Ophthal. Physiol. Opt. **21**, 393-400 (2001).

9. J. A. M. Jennings and W. N. Charman, "Optical image quality in the peripheral retina. Amer. J. Optom. Physiol. Opt. **55**, 582-590 (1978).

10. J. A. M. Jennings and W. N. Charman, "Off-axis image quality in the human eye," Vision Res. **21**, 445-455 (1981).

11. D. R. Williams, P. Artal, R. Navarro, M. J. McMahon and D. H. Brainard, "Off-axis optical quality and retinal sampling in the human eye," Vision Res. **36**, 1103-1114 (1996).

12. J.A. M. Jennings and W. N. Charman, "Analytic approximation of the off-axis modulation transfer function of the eye," Ophthal. Physiol. Opt. **17**, 697-704 (1997).

13. R. Navarro, E. Moreno and C. Dorronsoro, "Monochromatic aberrations and point-spread functions of the human eye across the visual field," J. Opt. Soc. Amer. A **15**, 2522-2529 (1998).

14. Standards Australia/Standards New Zealand, "Laser Safety. Part 1: Equipment classification, requirements and user's guide," (1997).

15. L. N. Thibos, R. A. Applegate, J. T. Schwiegerling, R. Webb and VSIA Standards Taskforce Members, "Report from the VSIA taskforce on standards for reporting optical aberrations of the eye," J. Refract. Surg. **16**, S654-S655 (2000).

16. R. Navarro, J. Santamaría and J. Bescós, "Accommodation-dependent model of the human eye with aspherics. J. Opt. Soc. Am. A **2**, 1273-1281 (1985).

17. I. Escudero-Sanz and R. Navarro, "Off-axis aberrations of a wide-angle schematic eye model," J. Opt. Soc. Am. A **16**, 1881-1891 (1999).

18. D. A. Atchison and G. Smith, "*Optics of the human eye*," Butterworth-Heinemann, Oxford, 147-149, 173-176 (2000).

FIGURE CAPTIONS

Figure 1. Apparatus for measuring aberrations of the eye. M_1, mirror; L_1-L_6 lenses; A_1 -A_3, apertures; PBS_1-PBS_3, pellicle beamsplitters.

Figure 2. Root-mean squared aberrations (waves) as a function of visual field angle for our subjects. All 2nd order results have been corrected for the on-axis defocus. a-e show 2nd to 6th orders for individual subjects. f shows only 3rd to 6th orders for the mean results. Note that the vertical scale is different in f than for the other figures. The error bars in f indicate standard deviations.

Figure 3. Root-mean squared aberrations (waves) as a function of visual field angle for a) the experimental study of Navarro *et al.*[13] along the nasal semi-meridian, and b) the Navarro model eye. The experimental results are the means and standard deviations for 4 subjects, except at 5° for which only 3 subjects were measured.
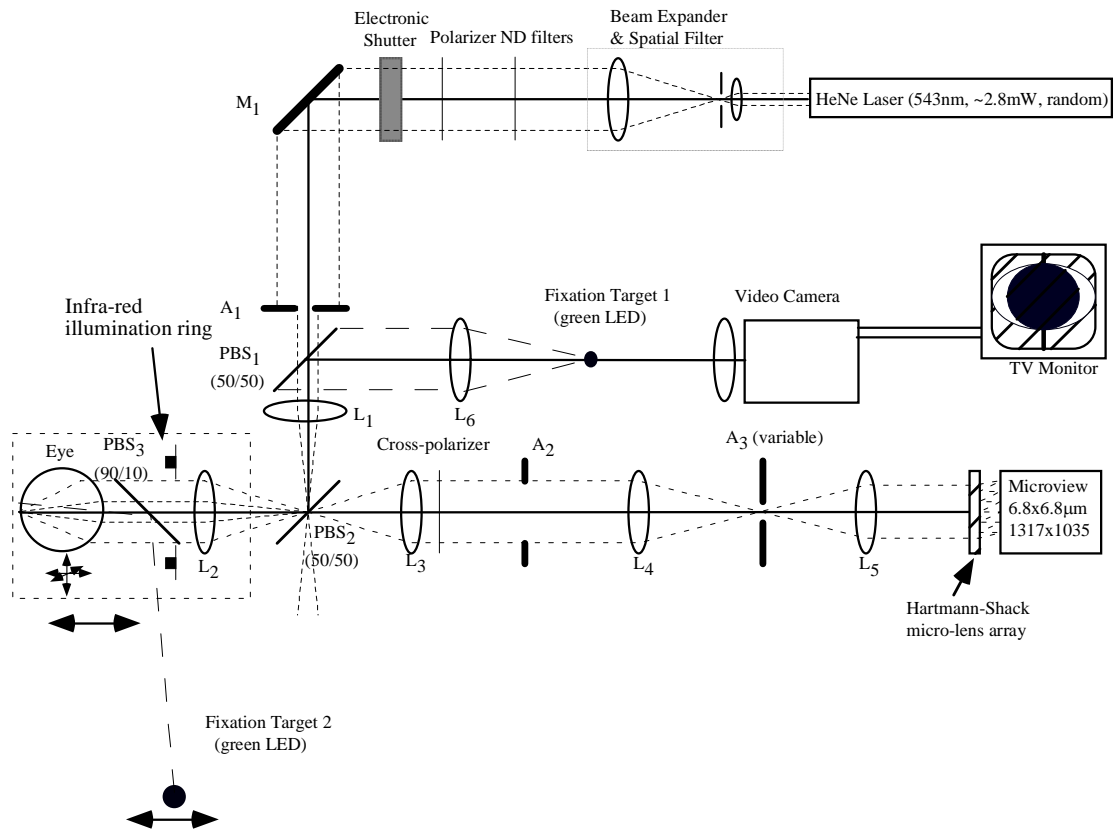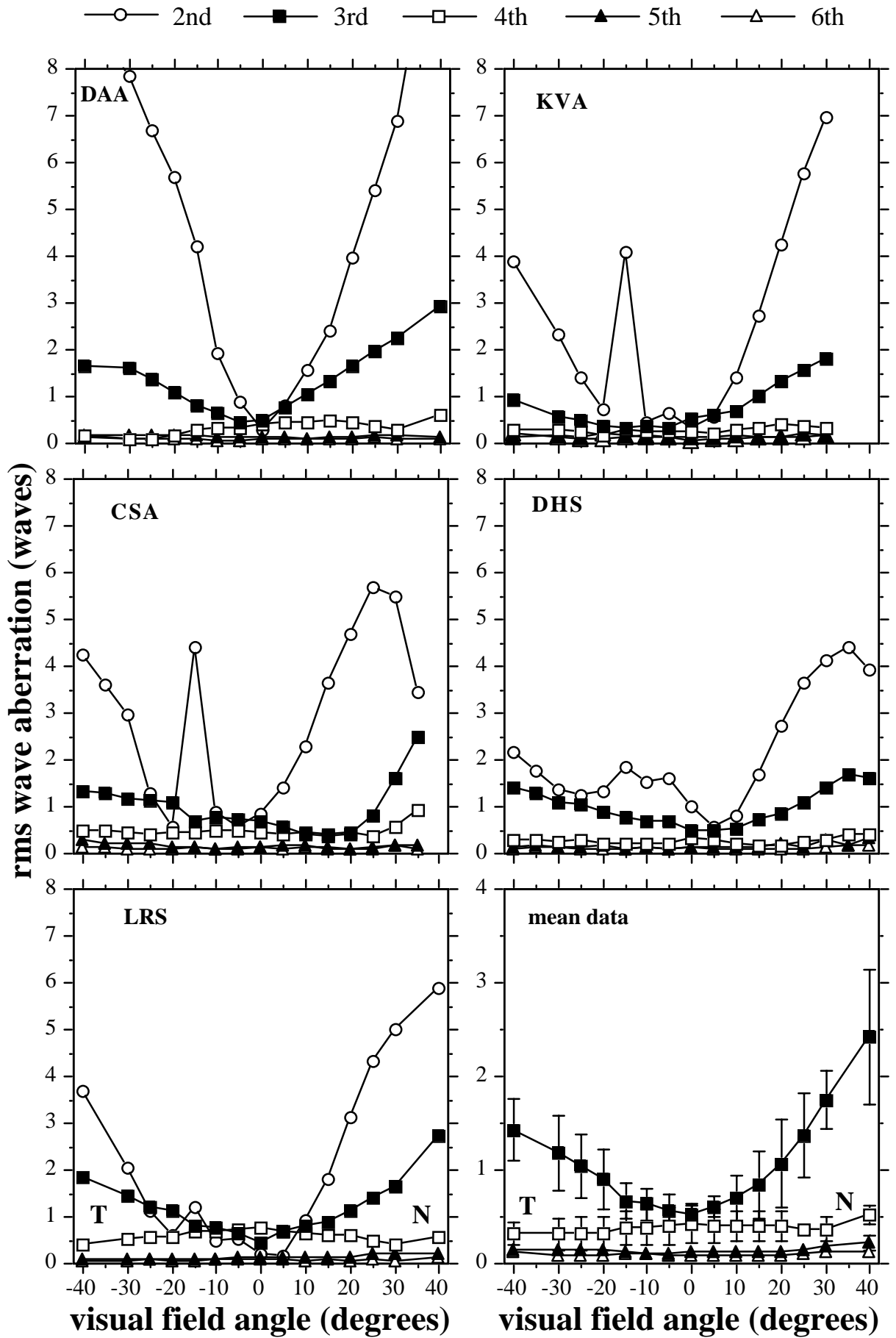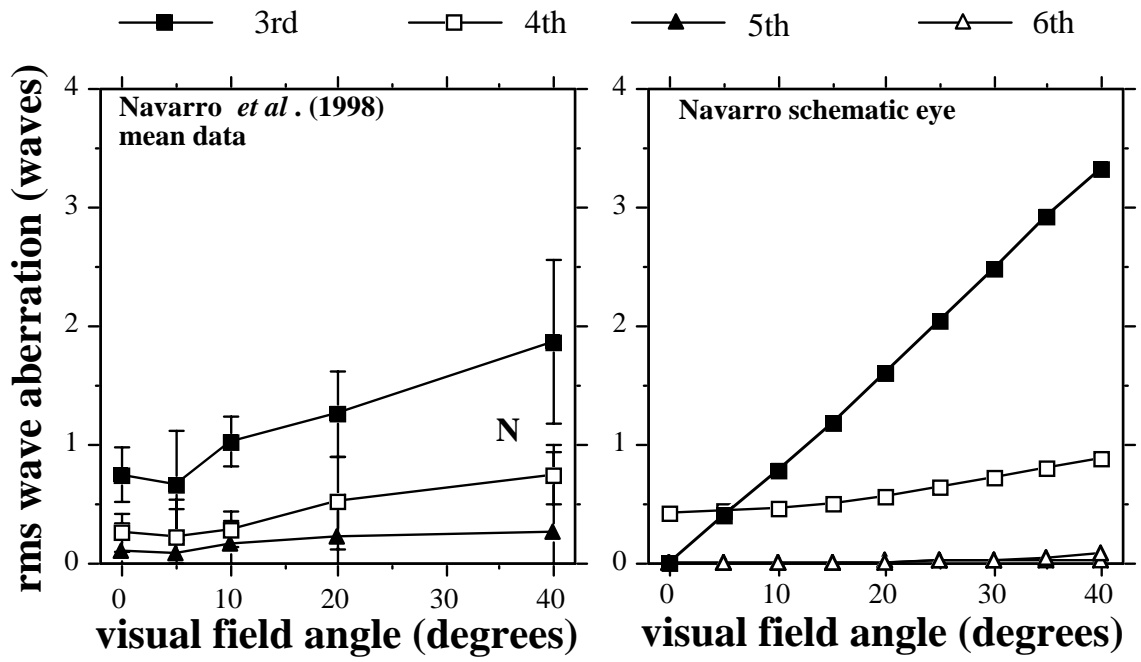
Figure 1

Figure 2

Figure 3